

Effect of iron on density and sound velocity of ringwoodite at high pressure and high temperature

Lei. Liu ^{a*}, Fengxia. Sun ^a, Chaowen. Xu ^a, Jianguo. Du ^a, Li. Yi ^a, Hong. Liu ^a,
Xxiaoyu. Gu ^a, Hanyu. Wang ^a, Gguangshu. Yang ^b

^a *United Laboratory of High-Pressure Physics and Earthquake Science, Institute of
Earthquake Forecasting, Key Laboratory of Earthquake Prediction, CEA, 100036,
Beijing, China*

^b *Faculty of Land Resources Engineering, Kunming University of Science and
Technology, 650093, Kunming, Yunnan, China*

1. Introduction

Iron is abundantly enriched in the mantle, usually substitutes magnesium in
mantle minerals (Zhang et al., 2019). It was found that the incorporation of iron in
silicate minerals modifies their physical properties (Ganskow et al., 2010; Higo et al.,
2006; Mao et al., 2006;). Compared with effect of temperature, the variation of iron
concentration in the cold subducting slab at mantle transition zone was more likely to
help explain the observed velocity anomalies (Ringwood and Irifune, 1988; Higo et
al., 2006; Ganskow et al., 2010; Jacobsen et al., 2004; Okuda et al., 2019; Zhang et al.,
2019). The occurrence state of iron in the deep Earth attracted much attentions (Muir

* Corresponding author: liulei@ief.ac.cn (L. Liu); 13888600582@163.com (G. Yang)

and Brodholt, 2020). Experiment found that the Fe-bearing bridgmanite ((Mg_{0.85}Fe_{0.15})SiO₃) lost Fe and disproportionate to a nearly Fe-free MgSiO₃ bridgmanite and Fe-rich phase H at 95-101GPa and 2200-2400K (Zhang et al., 2014). The experiments showed that Fe²⁺ in the deep magma ocean disproportionately forms Fe³⁺ and metallic iron at high pressures. It is reported that the reduced metallic iron sinks to the core and leaves an oxidized mantle that leads to the degasification of carbon dioxide and water from the mantle (Armstrong et al., 2019).

Ringwoodite is a high-pressure polymorph of olivine with the spinel-structured (Mg,Fe)₂SiO₄, and is considered to be the major constituent mineral of the Earth's mantle between depths of 510 and 660 km (Ringwood and Irifune, 1988). The pyrolitic mantle is mainly composed of ~60% ringwoodite and ~40% majoritic garnet at conditions of the lower part of the mantle transition zone (Hirose, 2002; Irifune, 1987). The velocity increase across the 410km, 520km and 660 km discontinuity may be caused by phase transition of olivine to its high pressure polymorphs (wadsleyite, ringwoodite) respectively (Matsui, 2001). Iron content of ringwoodite is suggested to be 10 at% (Higo et al., 2008). Thus, the properties of Fe-bearing- ringwoodite under high pressure and high temperature are important to understand the structure and composition of the mantle. So knowledge of structural and thermoelastic properties of ringwoodite have been widely studied: thermal expansion at high-temperatures (Suzuki et al., 2009), room temperature compressibility (Hazen, 1993; Zerr et al., 1993), sound velocities at various pressures and temperatures (Weidner et al., 1984; Sinogeikin et al., 1997, 1998, 2001; Jackson

et al., 2000; Katsura et al., 2004; Higo et al., 2004, 2006; Valdez et al., 2011, 2012; Rigden and Jackson, 1991; Rigden et al., 1991, 1992; Sinogeikin et al., 2001, Li et al., 2003). It is indicated that iron significantly affects the density and velocity of ringwoodite.

Theoretical calculations, e.g. the First-principle calculations, play a more effective role in studying material properties under the high pressure and temperature conditions because of rapid increasing of computational power. The First-principle methods are successfully used to simulate the Earth and planetary materials at high pressures and temperatures (Wentzcovitch and Stixrude, 2010; Jahn and Kowalski, 2014). Precisely determining effect of iron substitution on the physical properties of candidate mantle materials can provide critical insights into the composition and dynamics of the mantle (Lin et al., 2007; Lay et al., 2008). Studies on density and velocity of bearing-Fe ringwoodite under the simultaneously high-pressure and high-temperature conditions are still limited (Sinogeikin et al., 2003). Therefore, this work present the density and sound velocity of the ringwoodite with different Fe concentrations (0, 12.5, 25, 50, and 100 at%) under 0-26 GPa and 300-2000 K by the First-principle methods.

2. Simulated Method

The calculations were performed by the General Utility Lattice Program (GULP) codes (Gale and Rohl, 2003). The ClayFF forcefield was used to describe potential energy surface due to interactions between bonded atoms (Cygan et al., 2004). The ringwoodite is cubic and exists in a γ -spinel structure that belongs to space group Fd-3m and includes 56 atoms in its unit cell (Hazen et al., 1993). The $2\times 2\times 2$ supercells are used in this work. The iron-bearing ringwoodites were constructed by substituting the magnesium in the pure-Mg phase with iron and 4 structures that contain 12.5, 25, 50 and 100 at% Fe were built. The molecular dynamic simulations were performed in the statistical ensemble of constant-pressure and constant temperature (NPT). The equilibrium time is 10 ps, the time step is 0.2 fs and the total production time is 100 ps for every calculation run.

3. Results

3.1 Benchmark calculations

The test calculations on lattice parameters and elastic properties of ringwoodite were carried out for assessing the performance of the forcefield combined with molecular dynamic approach used here. The calculated density (ρ), bulk modulus (K), shear modulus (G), compressional wave velocities (V_p), and shear wave velocities (V_s) are listed in Table 1 together with the previous data at ambient conditions for comparison.

Table 1 The density and elastic properties of ringwoodite at ambient condition

Composition	Density	K	G	Vp	Vs	Conditions	Reference
	g/cm ³	GPa		km/s			
Mg ₂ SiO ₄	3.515	185	120	9.86	5.78	ambient	Li,et al., 2003
	3.515	184	120	9.75	5.82	ambient	Rigden,et al.,1991
		190	125	9.93	5.87	0GPa, 0K	Kiefer,et al.,1997
	3.559	185	120	9.85	5.82	ambient	Jackson,et al.,2000
	3.559	184	119	9.86	5.78	ambient	Weidner,et al.,1984
	3.572	185	127	9.96	5.93	ambient	Higo, et al., 2006
	3.61	196.5	124.7	10	5.9	0GPa, 0K	Nunez-Valdez, et al.,2011
	3.501	218.6	120.8	10.43	5.89	300K, 0GPa	This work
Mean differences (%)	-1.4%	+16.6%	-0.5%	+5.6%	+1.1%		
(Mg _{0.91} Fe _{0.09}) ₂ SiO ₄	3.69	186	119	9.66	5.68	ambient	Y.Higo,2008
	3.701	188.2	119.5	9.69	5.68	0.05GPa,295K	Sinogeikient, et al. 1998
	3.702	187.6	120.6	9.70	5.71	0GPa, 295K	Sinogeikient, et al. 2003
(Mg _{0.75} Fe _{0.25}) ₂ SiO ₄	3.878	193	113	9.39	5.4	ambient	Sinogeikient, et al.,1997
(Mg _{0.5} Fe _{0.5}) ₂ SiO ₄	4.176	191	102	8.85	4.94	ambient	Higo, et al., 2006
(Mg _{0.875} Fe _{0.125}) ₂ SiO ₄	3.70	197.1	120.5	9.7	5.6	0GPa, 0K	Nunez-Valdez, et al.,2011
	3.581	222.1	121.1	10.35	5.82	300K, 0GPa	This work
Mean differences (%)	-3.2%	+12.7%	-0.5%	+6.7%	+3.9%		

Our derived values of density, G and V_s are agreement well with previous results at ambient condition (Li, et al., 2003; Rigden,et al.,199; Kiefer,et al.,1997; Jackson, et al.,2000; Weidner, et al.,1984; Higo, et al., 2006, 2008; Nunez-Valdez, et al., 2011; Sinogeikient, et al., 1997, 1998, 2003), the mean difference are between 0.5% and 3.9%. The K and V_p , are respectively 5.6-6.7% and 12.7-16.6% larger than that of previous results.

To further verify validity of our used calculated approach, the density, V_p and V_s of ringwoodite with different Fe content under high pressure and temperature are also compared with previous results. The results are presented in Figure 1, 2 and 3.

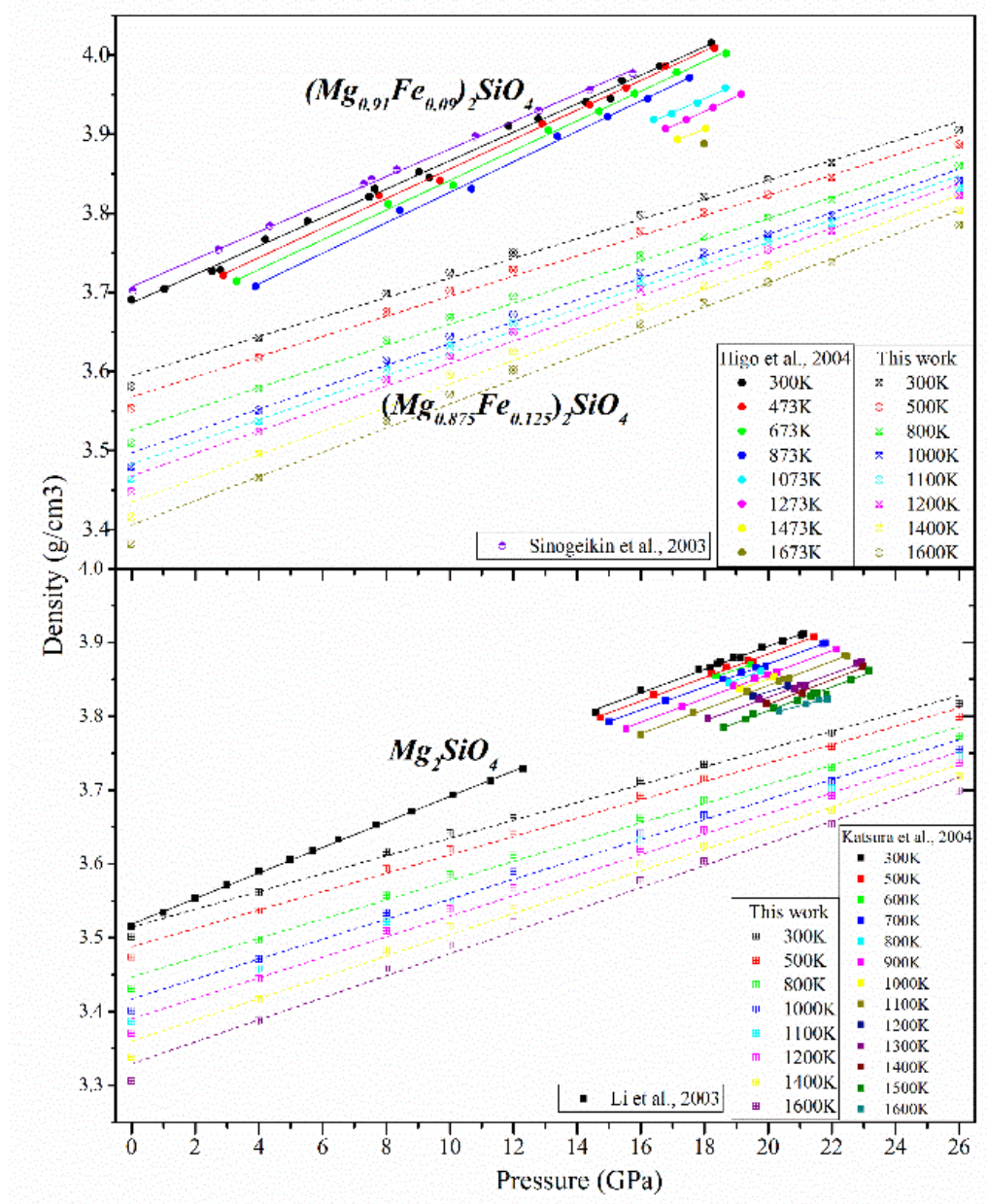


Figure 1. Density of ringwoodite with various Fe content at high pressure and temperature

Densities of Mg-endmember and Fe-bearing ringwoodite at 0-26 GPa and 300-1600K are shown in Figure 1. Higo et al. (2003) presented the density of ringwoodite with 10 wt% Fe. Our calculated densities are smaller than previous results up to 5.1% (Li et al., 2003; Sinogeikin et al., 2003; Katsura et al., 2004; Higo

et al., 2004). The differences are slight in the low pressure and become larger with increasing pressure.

As shown in Figure 2 and 3, all our calculated velocities are larger than previous results (Jackson et al., 2000; Li et al., 2003; Higo et al., 2006; Valdez et al., 2012). The V_p and V_s of Mg-endmember ringwoodite is respectively $\sim 6.8\%$ and $\sim 1.4\%$ larger than the reported results of Li et al. (2003) and Higo et al. (2006) at 0-16 GPa and room temperature (Figure 2). Besides, the V_p and V_s of pure-Mg ringwoodite is respectively $\sim 5.2\%$ and 1.1% larger than the reported results of Jackson et al. (2000) at 298-873K GPa and room pressure. Valdez et al. (2012) calculated V_p and V_s of pure-Mg ringwoodite at 0-30 GPa and 300-3000K by density functional theory (DFT) and quasi-harmonic approximation (QHA) simulation (Figure 2). The velocity contrast ΔV_p and ΔV_s between ours and those reported by Valdez et al. (2012) is less than 10.2% and 8.1%, respectively.

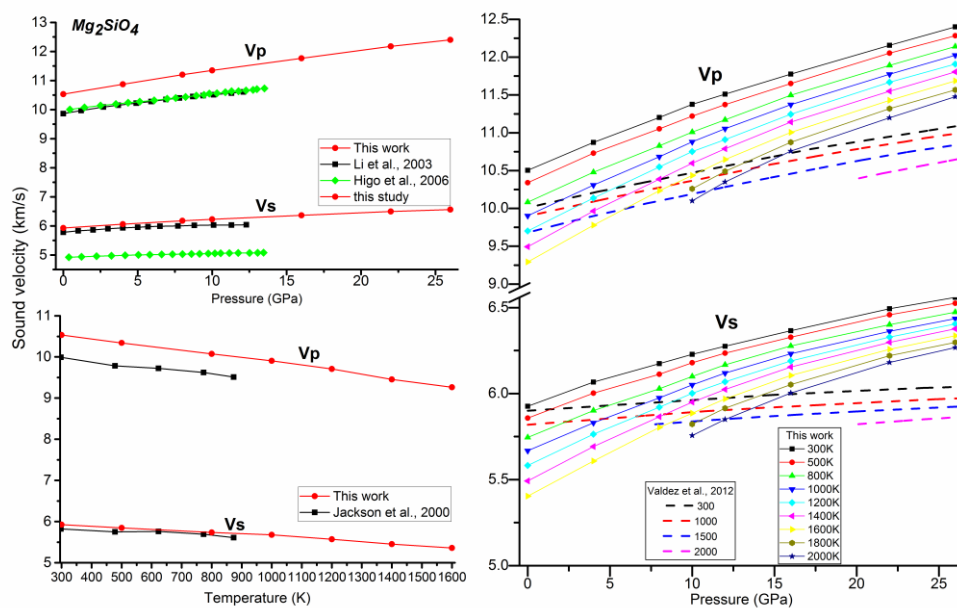


Figure 2 Comparison of velocity of Mg-endmember ringwoodite at high pressure and temperature

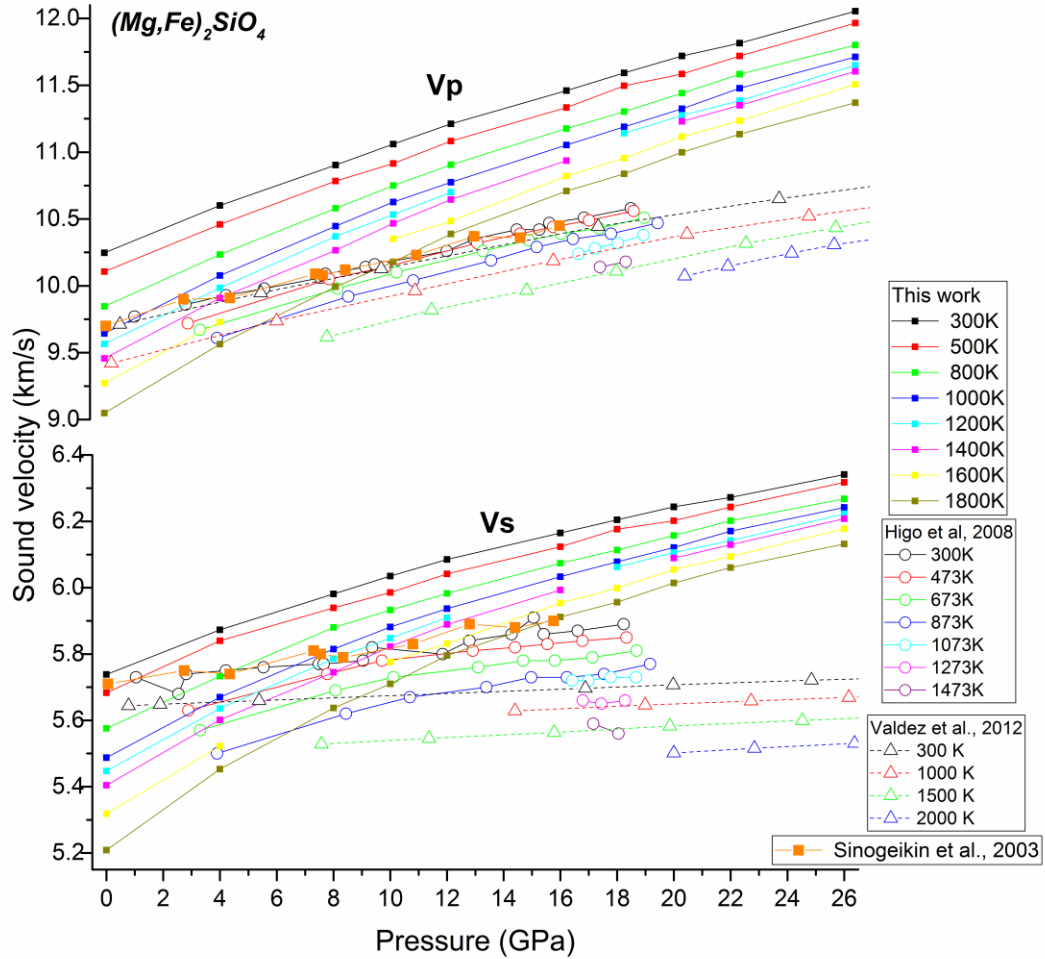


Figure 3 Comparison of velocity of Fe-bearing ringwoodite at high pressure and temperature

The comparisons of Vp and Vs of Fe-bearing ringwoodite with earlier studies are plotted in the Figure 3. Three works are used to be compared with our calculated $(\text{Mg}_{0.875}\text{Fe}_{0.125})_2\text{SiO}_4$ including the $(\text{Mg}_{0.875}\text{Fe}_{0.125})_2\text{SiO}_4$ (0-30 GPa and 300-3000K, Valdez et al., 2012), $(\text{Mg}_{0.91}\text{Fe}_{0.09})_2\text{SiO}_4$ (0-19.16 GPa and 300-1473K, Higo et al.,

2006) and $(\text{Mg}_{0.91}\text{Fe}_{0.09})_2\text{SiO}_4$ (0.05-15.76 GPa and room temperature, Sinogeikin, et al., 2003). The ΔV_p and ΔV_s between our calculated results and previous results (Valdez et al., 2012; Higo et al., 2006; Sinogeikin et al., 2003) increase with increasing pressure, up to 8.7% and 5.1%, respectively.

In general, compared with the previous results, our calculated values of density are smaller, K is larger, G is similar, and all V_p and V_s are larger. The biggest differences of density, V_p and V_s between our calculated results and previous results (Mg-endmember and Fe-bearing phase included) are 5.1%, 10.2% and 8.1% at range of 0-26 GPa and 300-2000K, respectively. At the same time, the differences increase with increasing pressure. Namely our calculated pressure gradients of density, V_p and V_s are larger than previous results. In a word, those results prove the validity of the calculated method used here for simulating the properties of ringwoodite under high pressure and high temperature.

3.2 The effect of Fe on density

Changes of the densities of ringwoodite with different Fe content under 0-26 GPa and 300-2000K are presented in Figure 4, Table 2 and supplementary table 1. The densities linearly increase with increasing Fe content and pressure; however linearly decrease with increasing temperature. The changes of density with pressure and temperature are fitted as follows:

$$\rho = \rho_0 + aT + bP,$$

where ρ and ρ_0 is the density (g/cm^3), P indicates pressure (GPa) and T indicates

the temperature (K), and a and b are fitting coefficient. The fitted results are shown in Table 2.

Table 2.Fitted coefficient of changes of density of ringwoodite with different Fe content

Fe content (at%)	0	12.5	25	50	100
ρ_0	3.528	3.609	3.689	3.848	4.783
a	-0.00011	-0.000113	-0.000114	-0.000117	-0.000131
b	0.01353	0.01386	0.01414	0.01472	0.01748

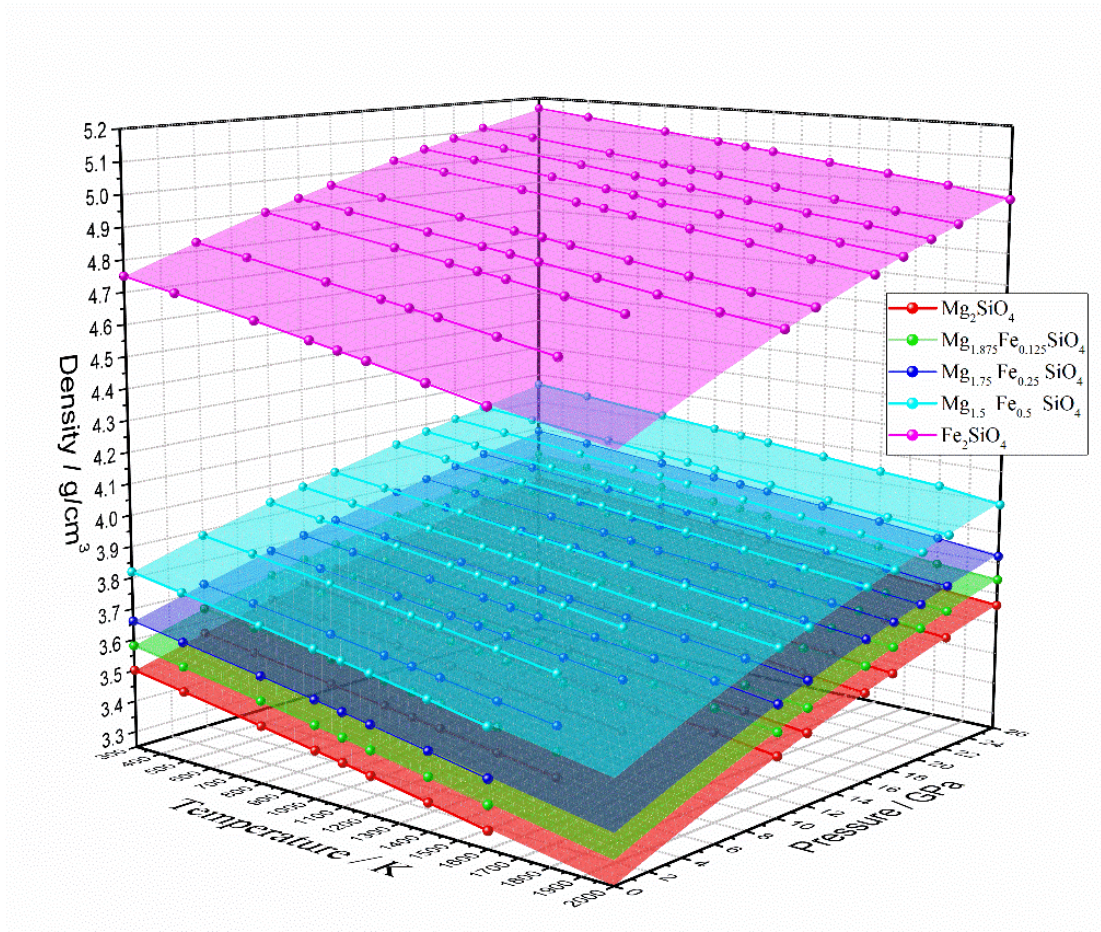
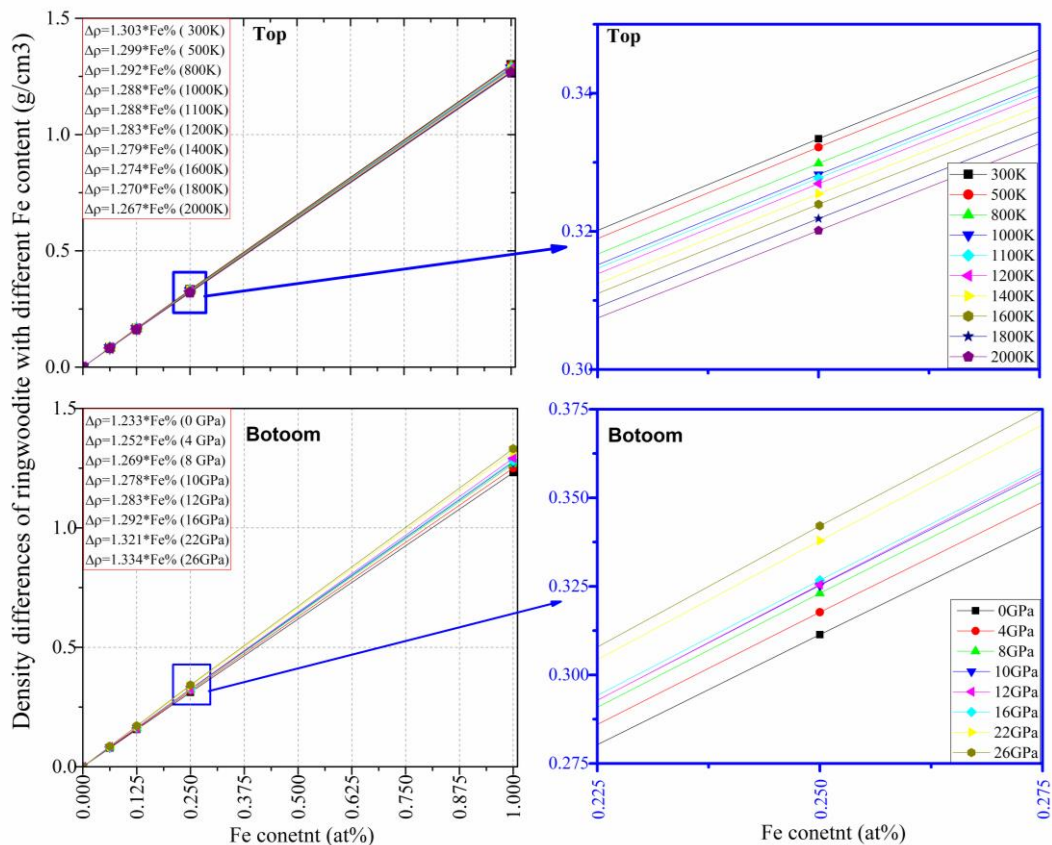


Figure 4 Densities of ringwoodite with different Fe content

155

156 To understand the quantitative effect of Fe, the comparison of Fe-bearing
 157 ringwoodite and Mg-endmember phase are shown in Figure 5. The differences
 158 between Fe-bearing ringwoodite and the Mg-endmember phase linearly increase with
 159 increasing Fe content. The fitted formula also listed in the Figure 5 under different
 160 pressure and temperature. The linear fitting coefficient decreases by 2.76% when
 161 temperature increasing from 300 K to 2000K, but increases by 8.19% when pressure
 162 increasing from 0 to 26 GPa.

163



164

165 Figure 5 Differences of density of Fe-bearing ringwoodite with the Mg-endmember phase
 166 under different Fe condition

167

3.3 The effect of Fe on Vp and Vs

Vp and Vs of ringwoodite under 0-26 GPa and 300-2000K are presented in Figure 6 and supplementary table 2. Both Vp and Vs decrease with increasing temperature and Fe content, but increase with increasing pressure. The fitted results of Vp and Vs as a function of pressure and temperature are shown in Table 3. We notice that fitting coefficients slightly decrease with increasing Fe content.

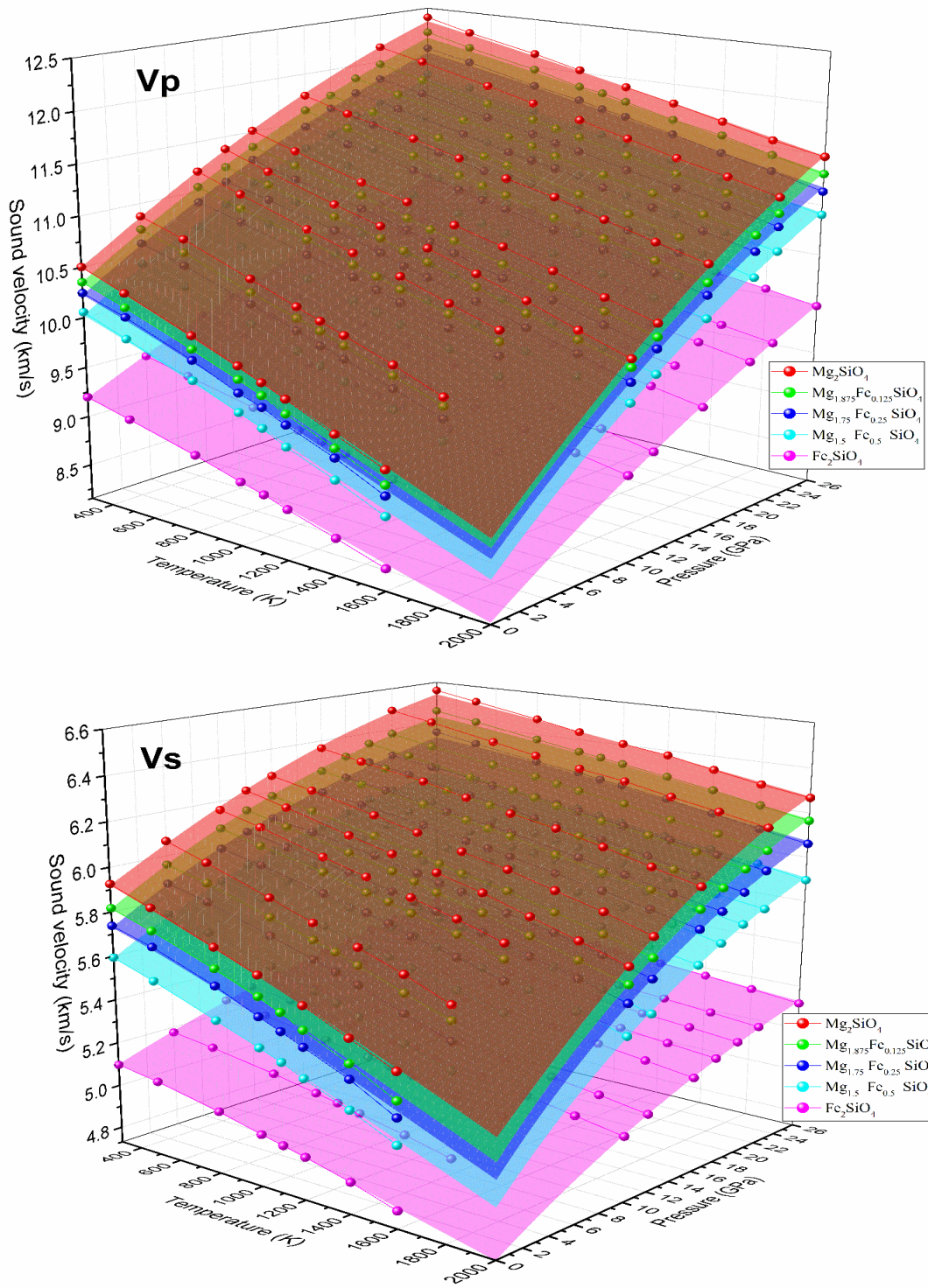


Figure 6 Sound velocity of ringwoodite with different Fe content under high pressure and temperature

Table 3. The fitted results of Vp and Vs as a function of pressure and temperature

Fe content (at%)	0	12.5	25	50	100
Vp					
Vp ₀	10.67	10.51	10.39	10.17	9.303
<i>a</i>	-0.000678	-0.000634	-0.000627	-0.000603	-0.000452
<i>b</i>	0.08184	0.07992	0.07837	0.07564	0.06099
Vs					
Vs ₀	5.963	5.858	5.772	5.624	5.122
<i>a</i>	-0.0002432	-0.0002264	-0.0002212	-0.0002091	-0.0001234
<i>b</i>	0.02998	0.02942	0.02856	0.02697	0.01746

Notes: The changes of Vp and Vs with pressure and temperature are fitted as follows: $V = V_0 + aT + bP$, where V and V₀ is the sound velocity (km/s), P indicates pressure (GPa) and T indicates the temperature (K), and *a* and *b* are fitting coefficient.

Changes of Vp and Vs (ΔV_p and ΔV_s) caused by variation of Fe content of ringwoodite are calculated by $(V_{\text{Fe-bearing}} - V_{\text{Mg-endmember}})/V_{\text{Mg-endmember}} \times 100\%$, where $V_{\text{Fe-bearing}}$ and $V_{\text{Mg-endmember}}$ indicate the V_p and V_s of Fe-bearing and Mg-endmember ringwoodite, respectively. The fitting results show well quadratic positive correlation and do not vary with pressure and temperature. The fitted results as follows:

$$\Delta V_p = 25.478 \times \text{Fe\%} - 11.238 \times (\text{Fe\%})^2$$

$$\Delta V_s = 20.842 \times \text{Fe\%} - 10.807 \times (\text{Fe\%})^2$$

where Fe% indicates the Fe content of ringwoodite with unit of at%.

Compared with V_p, V_s is more influenced by the Fe. For example, V_p and V_s of ringwoodite containing 12.5at% Fe are respectively 2.56% and 3.06% smaller than that velocity of Mg-endmember ringwoodite.

4. Discussion

As the most abundant constitute mineral of lower part of the mantle transition zone (Bass and Anderson, 1984; Hirose, 2002; Irifune, 1987), the density and sound velocity of ringwoodite are important to understand the composition and structure of the mantle, those properties are also useful to deduce the content of ringwoodite and Fe in the mantle.

According to above fitted results, the density of ringwoodite with different Fe content at lower part of the mantle transition zone conditions (along the Earth's temperature profile and pressure gradient) are plotted in Figure 7. The densities of Mg-endmember ringwoodite and those containing 12.5, 25 and 50 at% Fe are lower than that of the typical Earth's density profile (PREM; Dziewonski and Anderson, 1981), but the density of Fe-endmember ringwoodite is higher. On base of our calculation, the Fe content of ringwoodite is estimated to be 55-64 at% to match the density of lower part of the mantle transition zone. More Fe is needed to be incorporated in ringwoodite to meet the density profile of the lower mantle. Compared with experimental results, our calculated density is lower. This may lead to underestimate Fe content of ringwoodite that needed to match the Earth's density profile. Study

214 showed that ringwoodite contains 10 at% Fe according to its low pressure polymorph
215 of the San Carlos olivine with a composition of $(\text{Mg}_{0.91}\text{Fe}_{0.09})_2\text{SiO}_4$ (Higo et al., 2008).
216 This content is much lower than that of 55-64%. Therefore, the existence of the
217 ringwoodite may result in a low-density region or gravity anomaly in the lower part of
218 the mantle transition zone (Chaves and Ussami, 2013; Bowin, 1983)

219

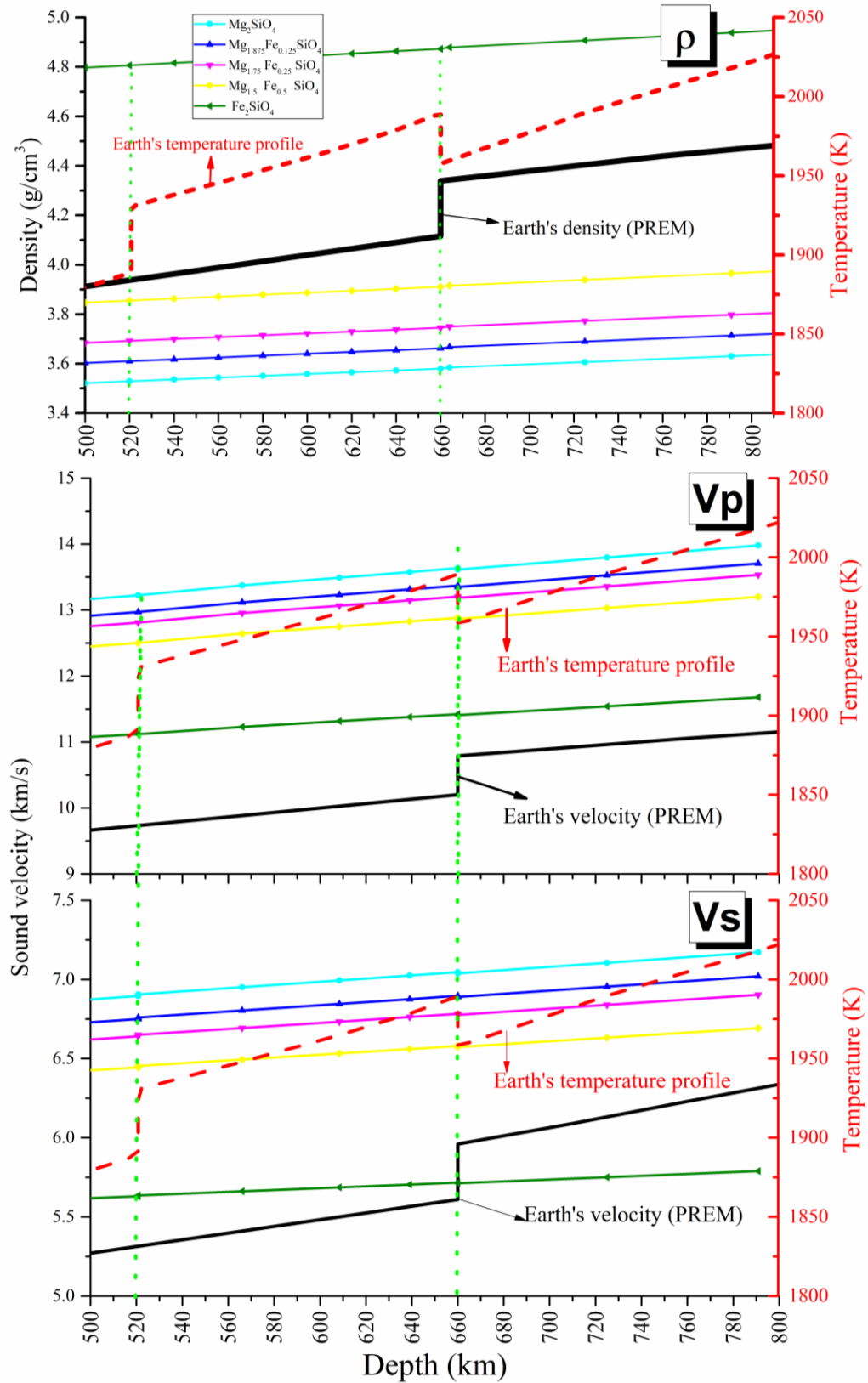


Figure 7 Density and sound velocity of ringwoodite along the Earth's temperature and pressure profile and comparison with the Earth's typical density model

223

224 The velocities obtained from seismic observation and those derived by
225 experiments and calculations can reflect the composition and structure of the Earth.
226 Thompson et al. (2017) showed that iron-enriched solid solutions in
227 FeOOH-AlOOH-MgSiH₂O₄ system contribute to the observed large low-shear
228 velocity provinces (LLSVP) in the lower mantle. Solid-state iron-enriched materials
229 (Mao et al., 2006; Deng, et al., 2019; Muira and Brodholt, 2020) have been proposed
230 to explain formation mechanism of the ultralow-velocity zones (ULVZs) at the
231 core-mantle boundary. The wave velocities of ringwoodite with different Fe content
232 under mantle transition zone condition are plotted in figure 7. The V_p and V_s of
233 ringwoodite along the Earth's typical temperature and pressure profile are higher than
234 that of the Earth's wave velocity model (Dziewonski and Anderson, 1981) at lower
235 part of the mantle transition zone (510-660 km). The V_p and V_s of ringwoodite with
236 12.5 at% Fe content are 31.3-33.7% and 22.9-27.7% higher. Even for the pure-Fe
237 ringwoodite, its V_p and V_s are still 12-14.7% and 1.9-6.5% higher. If ringwoodite can
238 enter the lower mantle, the V_s of pure-Fe ringwoodite would lower than the PREM
239 model, however the V_p of ringwoodite are still higher.

240 Ringwoodite will transform to bridgmanite+magnesiowüstite and then to
241 post-pervoskite at the lower mantle condition (Murakami et al., 2004; Tsuchiya et al.,
242 2004; Irifune et al., 1998; Ringwood, 1991). Experiment found that Fe-bearing
243 bridgmanite ((Mg_{0.85}Fe_{0.15})SiO₃) lost Fe and disproportionated to a nearly Fe-free
244 MgSiO₃ bridgmanite and an Fe-rich phase H at 95-101GPa pressure and 2200-2400K

temperature (Zhang et al., 2014). Fe^{2+} ions in the deep magma ocean disproportionate to form Fe^{3+} ions and metallic iron at high pressures, and the reduced metallic iron sinks to the core and leaves an oxidized mantle that leads to the degasification of carbon dioxide and water from the mantle (Armstrong et al., 2019). Therefore Fe content and the properties of Fe-bearing ringwoodite is important to explore structure, composition and dynamic process of the mantle. Our calculated quantitative equations of Fe effect provide the information to constrain the Fe content of the deep Earth and help to understand the effect of Fe on evolution of the Earth.

5. Conclusion

The density, V_p and V_s of ringwoodite with different Fe content (0, 12.5, 25, 50, and 100 at%) under 300-2000K and 0-26 GPa were calculated by forcefield combined with molecular dynamic method. This method is verified here to be effective in simulating physical properties of minerals. Changes of density, V_p and V_s of ringwoodite with pressure and temperature were fitted and presented. Density of ringwoodite linearly increases with increasing Fe content, however relationship between decrease of velocity and increasing Fe content show quadratic. Our calculated densities of ringwoodite show that the Fe content of ringwoodite shall be 55-64 at% to match the lower mantle transition zone's density. The existence of the ringwoodite may result in a low-density zone or gravity anomaly in the lower part of the mantle transition zone. The V_p and V_s of ringwoodite along the Earth's typical temperature and pressure profile are higher than the Earth's velocity. As the most important composition of lower mantle transition zone, the properties of Fe-bearing

ringwoodite under high pressure and high temperature are significant to explore Fe content and composition of the mantle.

Acknowledgments

This work was supported by the Special Fund of the Institute of Earthquake Forecasting, China Earthquake Administration(Grant No. 2019IEF0101-1, 2019IEF0502, 2017KLEP03) and The Opening Foundation of the United Laboratory of High-Pressure Physics and Earthquake Science (Grant No. 2019HPPE06); and by the National Natural Science Foundation of China (Grant No.41762008). Datasets for this research are available in these in-text data citation references: Liu L., 2020. doi: 10.17632/xf2rktzfgw.1).

References:

1. Armstrong, K., McCammon, C.A., Rubie, D.C., Ballaran, T.B. (2019). Deep magma ocean formation set the oxidation state of Earth's mantle. *Science*, 365 (6456), 903-906.<https://doi.org/10.1126/science.aax8376>
2. Bowin, C. (1983). Depth of principal mass anomalies contributing to the earth's geoidal undulations and gravity anomalies. *Marine Geodesy*, 7, 61–100. <https://doi.org/10.1080/15210608309379476>
3. Chaves, C.A.M., Ussami, N., (2013). Modeling 3-D density distribution in the mantle from inversion of geoid anomalies: Application to the Yellowstone Province. *Journal of Geophysical Research Solid Earth*, 118, 6328–6351.<https://doi.org/10.1002/2013JB010168>
4. Deng, J., Karki, B.B., Ghosh, D.B., Lee, K.K.M. (2019). First-principles study of FeO₂Hx

- 289 solid and melt system at high pressures: Implications for ultralow-velocity zones. *J. Geophys.*
290 *Res. Solid Earth*, 124, 4566-4575 . <https://doi.org/10.1029/2019JB017376>
- 291 5. Dziewonski, A.M., Anderson, D.L. (1981). Preliminary Reference Earth Model (PREM).
292 *Physics of the Earth & Planetary Interiors*, 25, 297-356.
293 [https://doi.org/10.1016/0031-9201\(81\)90046-7](https://doi.org/10.1016/0031-9201(81)90046-7)
- 294 6. Gale, J.D., Rohl, A.L. (2003). The general utility lattice program. *Molecular Simulation*,
295 29(5), 291-341. <https://doi.org/10.1080/0892702031000104887>
- 296 7. Ganskow, G., Ballaran, T.B., Langenhorst, F. (2010). Effect of iron on the compressibility of
297 hydrous ringwoodite. *American Mineralogist*, 95, 747-753.
298 <https://doi.org/10.2138/am.2010.3420>
- 299 8. Hazen, R.M., Downs, R.T., Finger, L.W., Ko, J. (1993). Crystal chemistry of ferromagnesian
300 silicate spinels: Evidence for Mg-Si disorder, *American Mineralogist*, 78, 1320 - 1323.
301 [https://doi.org/doi:10.1016/0892-6875\(93\)90105-V](https://doi.org/doi:10.1016/0892-6875(93)90105-V)
- 302 9. Hazen, R.M. (1993). Comparative compressibilities of silicate spinels: anomalous behavior
303 of (Mg, Fe)₂SiO₄. *Science*, 259, 206-209. <https://doi.org/10.1126/science.259.5092.206>
- 304 10. Hazen, R.M., Weinberger, M.B., Yang, H., Prewitt, C.T. (2000). Comparative high pressure
305 crystal chemistry of wadsleyite, β -(Mg_{1-x}Fe_x)₂SiO₄, with x=0 and 0.25, *American*
306 *Mineralogist*, 85, 770-777. <https://doi.org/10.2138/am-2000-5-617>
- 307 11. Higo, Y., Inoue, T., Irifune, T., Funakoshi, K.I., Li, B. (2008). Elastic wave velocities of
308 (Mg_{0.91}Fe_{0.09})₂SiO₄ ringwoodite under P-T conditions of the mantle transition region. *Physics*
309 *of the Earth & Planetary Interiors*, 166, 167-174. <https://doi.org/10.1016/j.pepi.2008.01.003>
- 310 12. Higo, Y., Inoue, T., Li, B., Irifune, T., Liebermann, R. (2006). The effect of iron on the elastic
311 properties of ringwoodite at high pressure. *Physics of the Earth & Planetary Interior*, 159,
312 276-285. <https://doi.org/10.1016/j.pepi.2006.08.004>
- 313 13. Hirose, K. (2002). Phase transitions in pyrolitic mantle around 670-km depth: implications
314 for upwelling of plumes from the lower mantle. *Journal of Geophysical Research Solid*

- 315 *Earth*, 107(B4), <https://doi.org/10.1029/2001JB000597>
- 316 14. Irifune, T. (1987). An experimental investigation of the pyroxene garnet transformation in a
317 pyrolite composition and its bearing on the constitution of the mantle. *Physics of the Earth &*
318 *Planetary Interiors*, 45, 324-336. [https://doi.org/10.1016/0031-9201\(87\)90040-9](https://doi.org/10.1016/0031-9201(87)90040-9)
- 319 15. Irifune, T., Nishiyama, N., Kuroda, K., Inoue, T., Isshiki, M., Utsumi, W., Funakoshi, K.,
320 Urakawa, S., Uchida, T., Katsura, T., Ohtaka, O. (1998). The postspinel phase boundary in
321 Mg_2SiO_4 determined by in situ X-ray diffraction. *Science*, 279, 1698-1700.
322 <https://doi.org/10.1126/science.279.5357.1698>
- 323 16. Jackson, J.M., Sinogeikin, S.V., and Bass, J.D. (2000). Sound velocities and elastic properties
324 of gamma- Mg_2SiO_4 to 873 K by Brillouin spectroscopy. *American Mineralogist*, 85, 296-303.
325 <https://doi.org/10.2138/am-2000-2-306>
- 326 17. Jacobsen, S.D., Smyth, J.R., Spetzler, H., Holl, C.M., Frost, D.J. (2004). Sound velocities and
327 elastic constants of iron bearing hydrous ringwoodite. *Physics of the Earth & Planetary*
328 *Interiors*, 143, 47-56. <https://doi.org/10.1016/j.pepi.2003.07.019>
- 329 18. Jahn, S., Kowalski, P. (2014). Theoretical approaches to structure and spectroscopy of earth
330 materials. *Reviews in Mineralogy & Geochemistry*, 78.
331 <https://doi.org/10.2138/rmg.2014.78.17>
- 332 19. Katsura, T., Yokoshi, S., Song, M., Kawabe, K., Funakoshi, K. I. (2004). Thermal expansion
333 of Mg_2SiO_4 ringwoodite at high pressures. *Journal of Geophysical Research Solid Earth*,
334 109(12), 221-232. <https://doi.org/10.1029/2004JB003094>
- 335 20. Kiefer, B., Stixrude, L., Wentzcovitch, R.M. (2013). Calculated elastic constants and
336 anisotropy of Mg_2SiO_4 spinel at high pressure. *Geophys. Research Letters*, 24, 2841-2844.
337 <https://doi.org/10.1029/97GL02975>
- 338 21. Komabayashi, T., Pesce, G., Sinmyo, R., Kawazoe, T., Breton, H., Shimoyama, Y. (2019).
339 Phase relations in the system Fe-Ni-Si to 200 GPa and 3900 K and implications for earth's
340 core. *Earth & Planetary Science Letters*, 512, 83-88.

- 341 <https://doi.org/10.1016/j.epsl.2019.01.056>
- 342 22. Lay, T., Hernlund, J., Buffett, B.A. (2008). Core-mantle boundary heat flow. *NATURE*
343 *GEOENCE*, 1(1), 25-32. <https://doi.org/10.1038/ngeo.2007.44>
- 344 23. Li., Baosheng. (2003). Compressional and shear wave velocities of ringwoodite γ - Mg_2SiO_4 to
345 12 gpa. *American Mineralogist*, 88-89, 1312-1317. <https://doi.org/10.2138/am-2003-8-913>
- 346 24. Lin, J.F., Vanko, G., Jacobsen, S.D., Lota, V., Struzhkin, V.V., Prakapenka, V.B. (2007). Spin
347 transition zone in earth's lower mantle. *Science*, 317(5845), 1740-1743.
348 <https://doi.org/10.1126/science.1144997>
- 349 25. Núñez-Valdez. M., Wu. Z., Yu. Y.G., Revenaugh, J., Wentzcovitch. R.M. (2012).
350 Thermoelastic properties of ringwoodite $(\text{Fe}_x\text{Mg}_{1-x})_2\text{SiO}_4$: its relationship to the 520 km
351 seismic discontinuity. *Earth & Planetary Science Letters*, 351-352.115-122.
352 <https://doi.org/10.1016/j.epsl.2012.07.024>
- 353 26. Núñez-Valdez, M., da Silveira, P., Wentzcovitch, R.M. (2011). Influence of iron on the elastic
354 properties of wadsleyite and ringwoodite. *Journal of Geophysical Research Solid Earth*, 116,
355 B12207. <https://doi.org/10.1029/2011JB008378>
- 356 27. Mao, W.L., Mao, H.K., Sturhahn, W., Zhao, J., Prakapenka, V.B., Meng, Y. (2006). Iron-rich
357 post-perovskite and the origin of ultralow-velocity zones. *Science*, 312(5773), 564-565.
358 <https://doi.org/10.1126/science.1123442>
- 359 28. Mashino, I., Miozzi, F., Hirose, K., Morard, G., Sinmyo, R. (2019). Melting experiments on
360 the Fe-C binary system up to 255 GPa: constraints on the carbon content in the earth's core.
361 *Earth & Planetary Science Letters*, 515, 135-144. <https://doi.org/10.1016/j.epsl.2019.03.020>
- 362 29. Matsui, M. (2001). Density and bulk sound velocity jumps across the 660 km seismic
363 discontinuity. *Physics of the Earth & Planetary Interiors*, 125, 141-146.
364 [https://doi.org/10.1016/S0031-9201\(01\)00235-7](https://doi.org/10.1016/S0031-9201(01)00235-7)
- 365 30. Murakami, M., Hirose, K., Kawamura, K., Sata, N., Ohishi, Y. (2004). Post-perovskite phase
366 transition in MgSiO_3 . *Science*, 304, 855-858. <https://doi.org/10.1126/science.1095932>

- 367 31. Muir, J.M.R., Brodholt, J.P. (2020). Ferric iron in bridgmanite and implications for ULVZs.
368 *Physics of the Earth & Planetary Interiors*, 306, 106505.
369 <https://doi.org/10.1016/j.pepi.2020.106505>
- 370 32. Okuda, Y., Ohta, K., Sinmyo, R., Takashi, K., Ohishi, Y. (2019). Effect of spin transition of
371 iron on the thermal conductivity of (Fe, Al)-bearing bridgmanite. *Earth & Planetary Science*
372 *Letters*, 520, 188-198. <https://doi.org/10.1016/j.epsl.2019.05.042>
- 373 33. Rigden, S.M., Gwanmesia, G.D., Fitz Gerald, J.D., Jackson, I., Liebermann, R.C. (1991).
374 Spinel elasticity and seismic structure of the transition zone of the mantle. *Nature*, 354,
375 143-145. <https://doi.org/10.1038/354143a0>
- 376 34. Rigden, S.M., Gwanmesia, G.D., Jackson, I., Liebermann, R.C. (1992). Progress in
377 high-pressure ultrasonic interferometry, the pressure dependence of elasticity of Mg₂SiO₄
378 polymorphs and constraints on the composition of the transition zone of the Earth's mantle.
379 In: Syono, Y., Manghnani, M.H. (Eds.), High- Pressure Research: Application to Earth and
380 Planetary Sciences. *American Geophysical Union, Washington, DC*, 167-182.
381 <https://doi.org/10.1029/GM067p0167>
- 382 35. Rigden, S.M., Jackson, I. (1991). Elasticity of germanate and silicate spinels at high pressure.
383 *Journal of Geophysical Research Solid Earth*, 96, 9999-10006.
384 <https://doi.org/10.1029/90JB02490>
- 385 36. Ringwood, A.E. (1991). Phase transformations and their bearing on the constitution and
386 dynamics of the mantle. *Geochimica et Cosmochimica Acta*, 55, 2083-2110.
387 [https://doi.org/10.1016/0016-7037\(91\)90090-R](https://doi.org/10.1016/0016-7037(91)90090-R)
- 388 37. Ringwood, A.E. and Irifune, T. (1988). Nature of the 650-km seismic discontinuity:
389 implications for mantle dynamics and differentiation. *Nature*, 331(6152), 131-136.
390 <https://doi.org/10.1038/331131a0>
- 391 38. Sinmyo, R., Hirose, K., Ohishi, Y. (2019). Melting curve of iron to 290 gpa determined in a
392 resistance-heated diamond-anvil cell. *Earth & Planetary Science Letters*, 510, 45-52.
393 <https://doi.org/10.1016/j.epsl.2019.01.006>

- 394 39. Sinogeikin, S.V., Bass, J.D., Katsura, T. (2003). Single-crystal elasticity of ringwoodite to
395 high pressures and high temperatures: implications for 520 km seismic discontinuity. *Physics*
396 *of the Earth & Planetary Interiors*, 136.1-2, 41-66.
397 [https://doi.org/10.1016/S0031-9201\(03\)00022-0](https://doi.org/10.1016/S0031-9201(03)00022-0)
- 398 40. Sinogeikin, S.V., Bass, J.D., Katsura, T. (2001). Single-crystal elasticity of
399 γ -(Mg_{0.91}Fe_{0.09})₂SiO₄ to high pressures and to high temperatures. *Geophysical Research*
400 *Letters*, 28, 4335-4338. <https://doi.org/10.1029/2001GL013843>
- 401 41. Sinogeikin, S.V., Bass, J.D., Kavner, A., Jeanloz, R. (1997). Elasticity of natural majorite and
402 ringwoodite from the Catherwood meteorite. *Geophysical Research Letters*, 24, 3265-3268.
403 <https://doi.org/10.1029/97GL03217>
- 404 42. Sinogeikin, S.V., Katsura, T., Bass, J.D. (1998). Sound velocities and elastic properties of
405 Fe-bearing wadsleyite and ringwoodite. *Journal of Geophysical Research Atmospheres*, 103,
406 20819-20825. <https://doi.org/10.1029/98JB01819>
- 407 43. Suzuki, I., Ohtani, E., Kumazawa, M. (2009). Thermal expansion of γ -Mg₂SiO₄. *Earth*
408 *Planets & Space*, 27, 53-61. <https://doi.org/10.4294/jpe1952.27.53>
- 409 44. Tsuchiya, T., Tsuchiya, J., Umemoto, K., Wentzcovitch, R.M. (2004). Phase transition in
410 MgSiO₃ perovskite in the Earth's lower mantle. *Earth & Planetary Science Letters*, 224,
411 241-248. <https://doi.org/10.1016/j.epsl.2004.05.017>
- 412 45. Weidner, D.J., Sawamoto, H., Sasaki, S., Kumazawa, M. (1984). Single-crystal elastic
413 properties of the spinel phase of Mg₂SiO₄. *Journal of Geophysical Research Solid Earth*, 89,
414 7852-7860. <https://doi.org/10.1029/JB089iB09p07852>
- 415 46. Wentzcovitch R M , Stixrude L . Theoretical and computational methods in mineral physics :
416 geophysical applications[M]. Mineralogical Society of America, 2010.
417 <https://doi.org/10.2138/rmg.2010.71>
- 418 47. Zerr, A., Reichmann, H., Euler, H., Boehler, R. (1993). Hydrostatic compression of
419 γ -(Mg_{0.6}, Fe_{0.4})₂SiO₄ to 50.0 GPa. *Physics & Chemistry of Minerals*, 19, 507-509.

420 <https://doi.org/10.1007/BF00203192>

421 48. Zhang, L., Meng, Y., Yang, W. (2014). Disproportionation of (Mg,Fe)SiO₃ perovskite in
422 Earth's deep lower mantle. *Science*, 344(6186), 877-882.

423 <https://doi.org/10.1126/science.1250274>

424 49. Zhang, Y., Yoshino, T., Yoneda, A., Osako, M. (2019). Effect of iron content on thermal
425 conductivity of olivine with implications for cooling history of rocky planets. *Earth &*

426 *Planetary Science Letters*, 519, 109-119. <https://doi.org/10.1016/j.epsl.2019.04.048>

427 50. Zhang, B., Yoshino, T., Zhao, C. (2019). The effect of water on Fe-Mg interdiffusion rates in
428 ringwoodite and implications for the electrical conductivity in the mantle transition zone.

429 *Journal of Geophysical Research Solid Earth*, 124, 2510-2524.

430 <https://doi.org/10.1029/2018JB016415>

431

Figure 1.

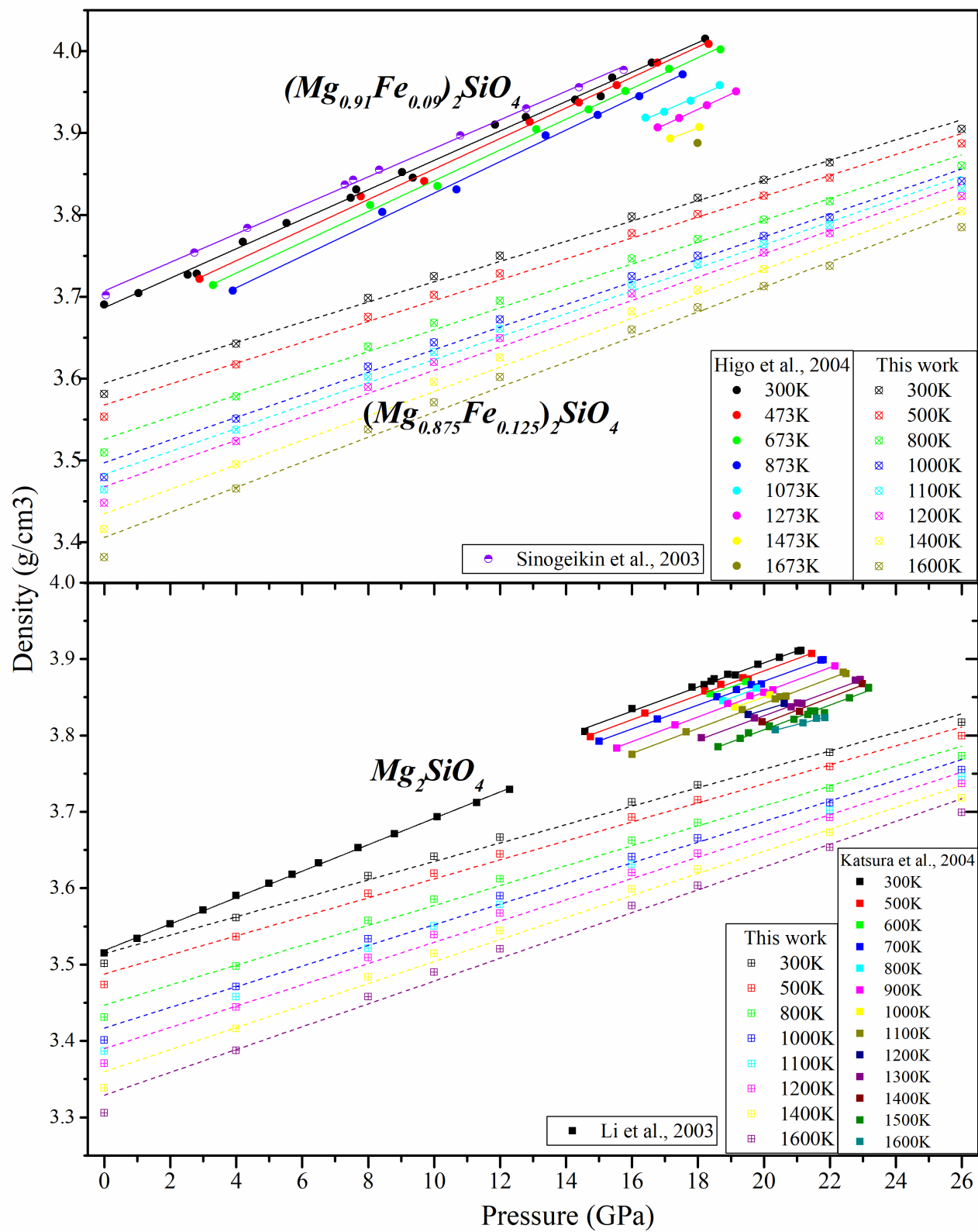


Figure 2.

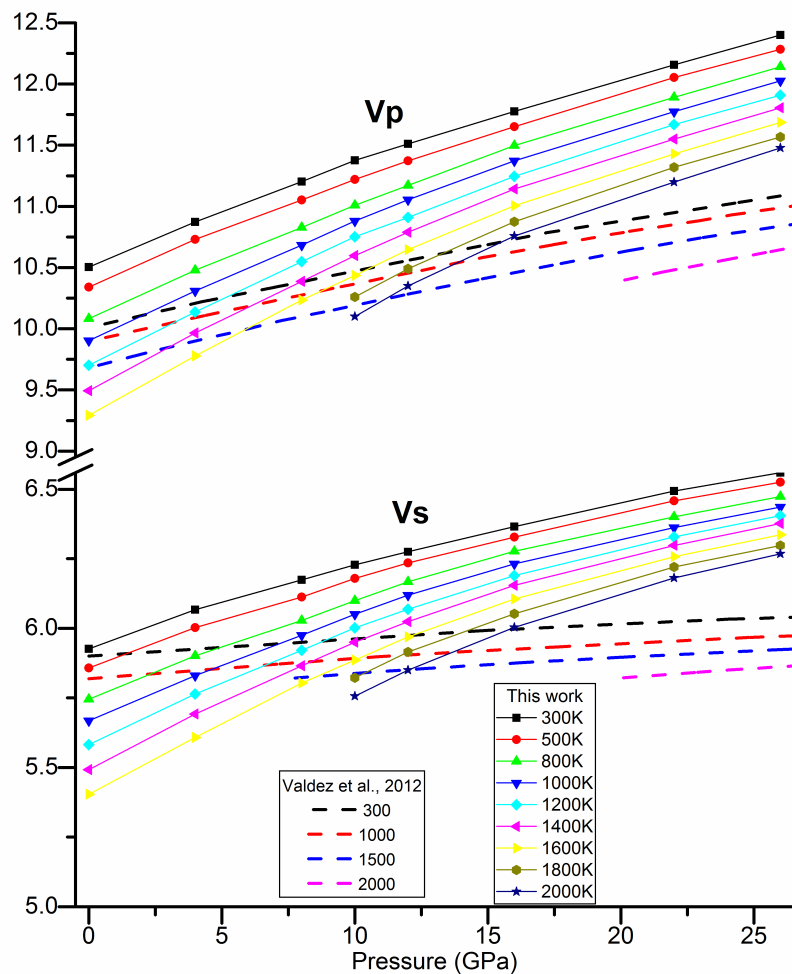
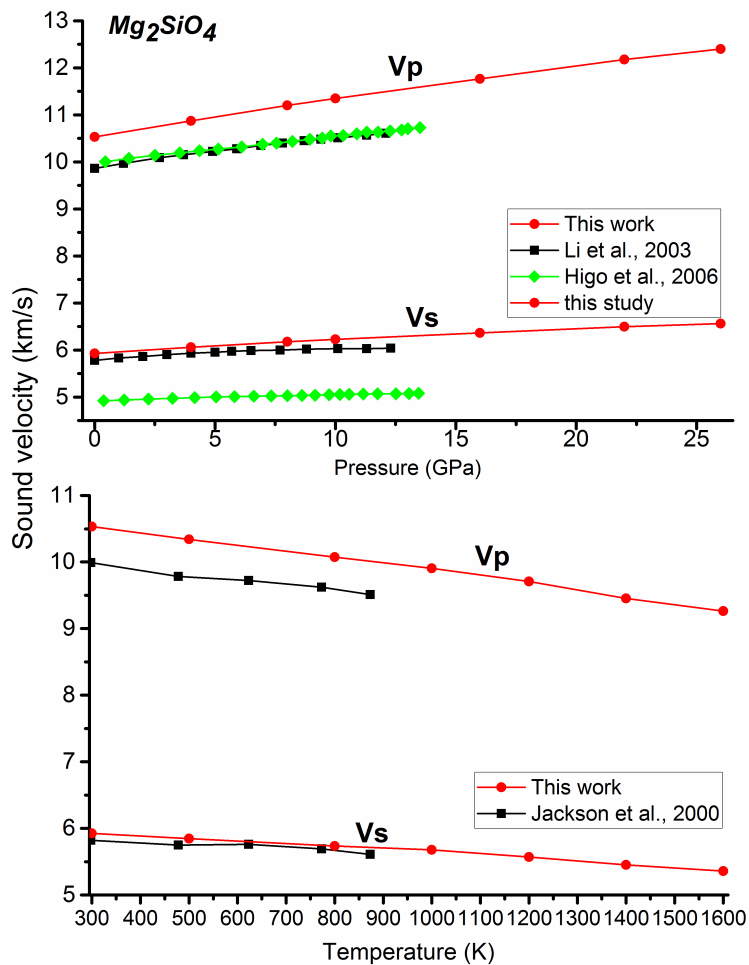


Figure 3.

$(\text{Mg,Fe})_2\text{SiO}_4$

V_p

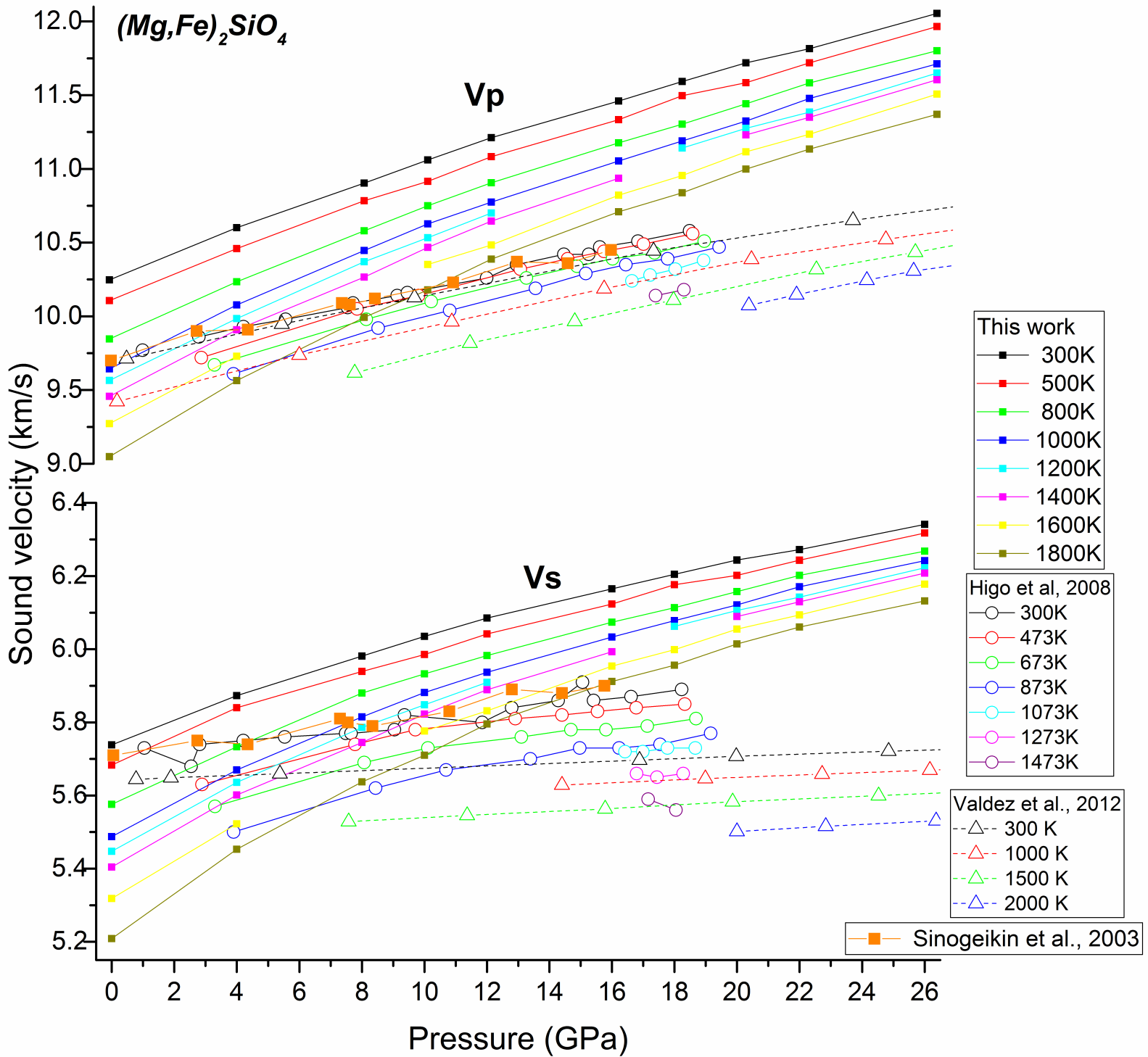


Figure 4.

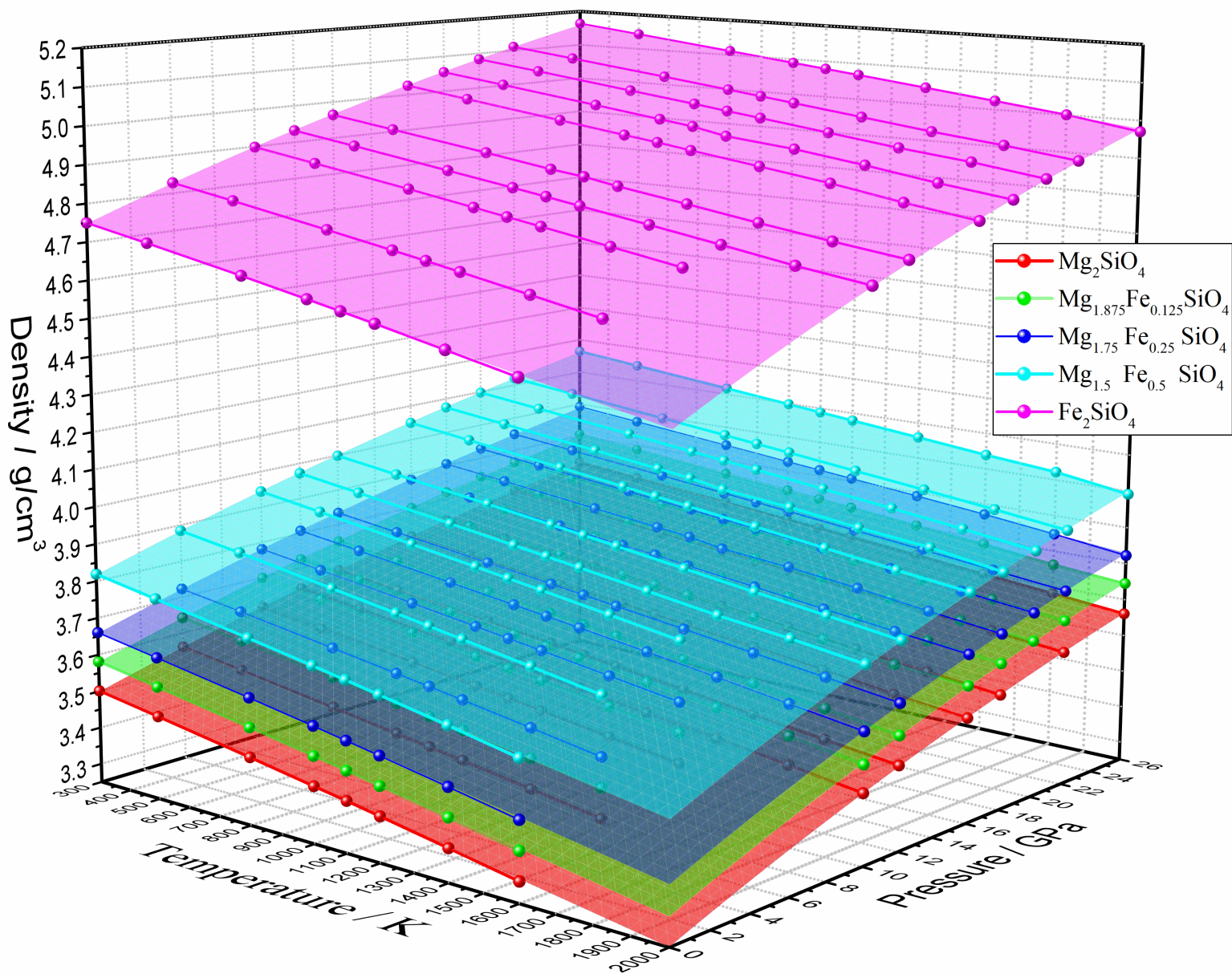


Figure 5.

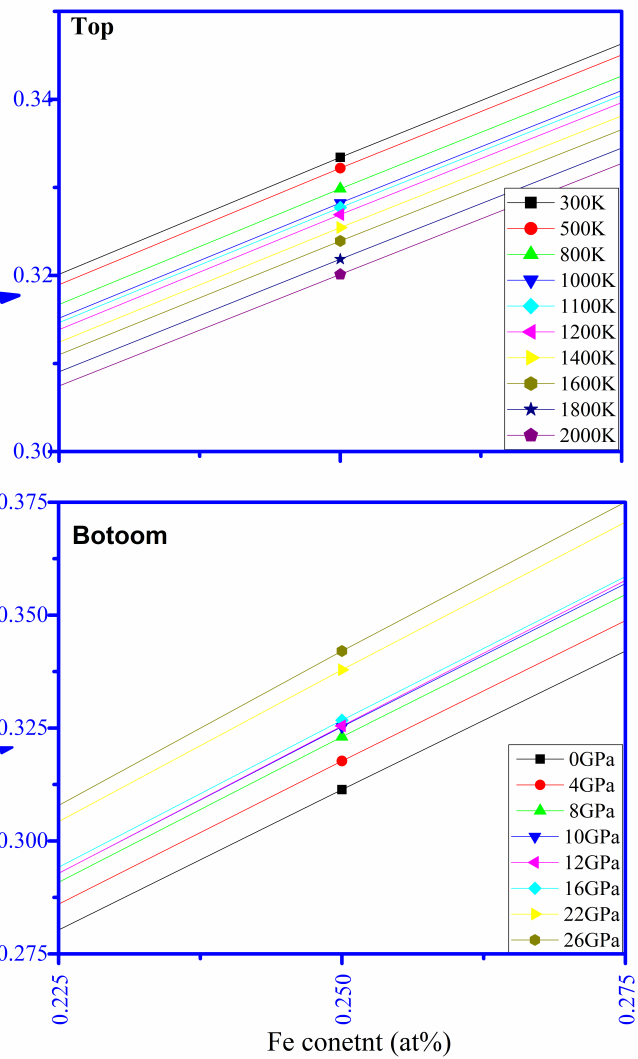
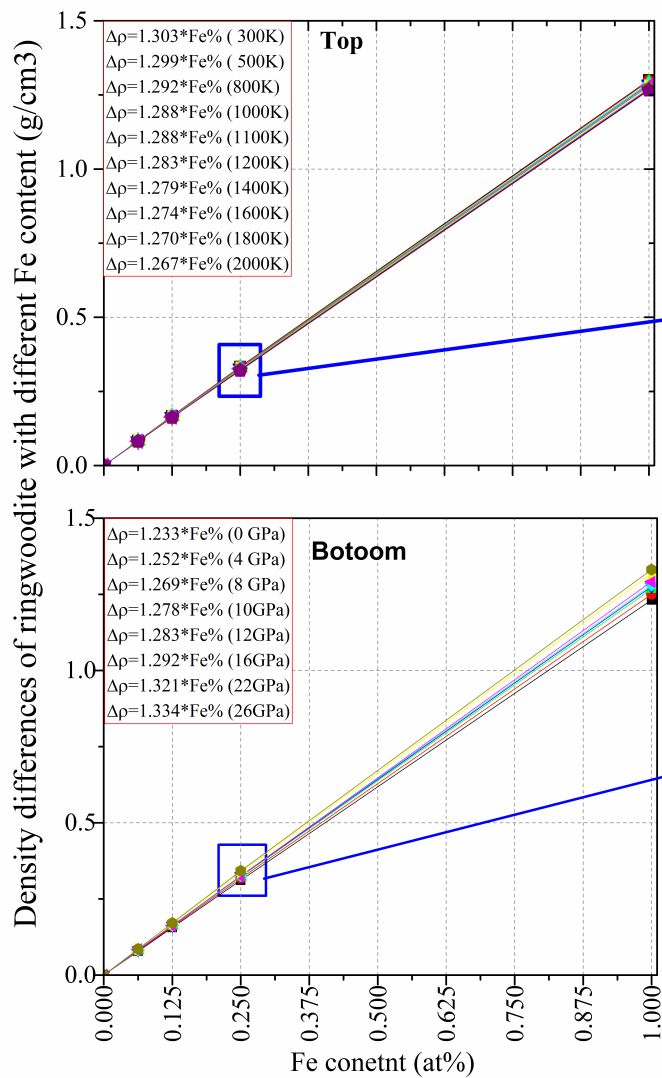


Figure 6.

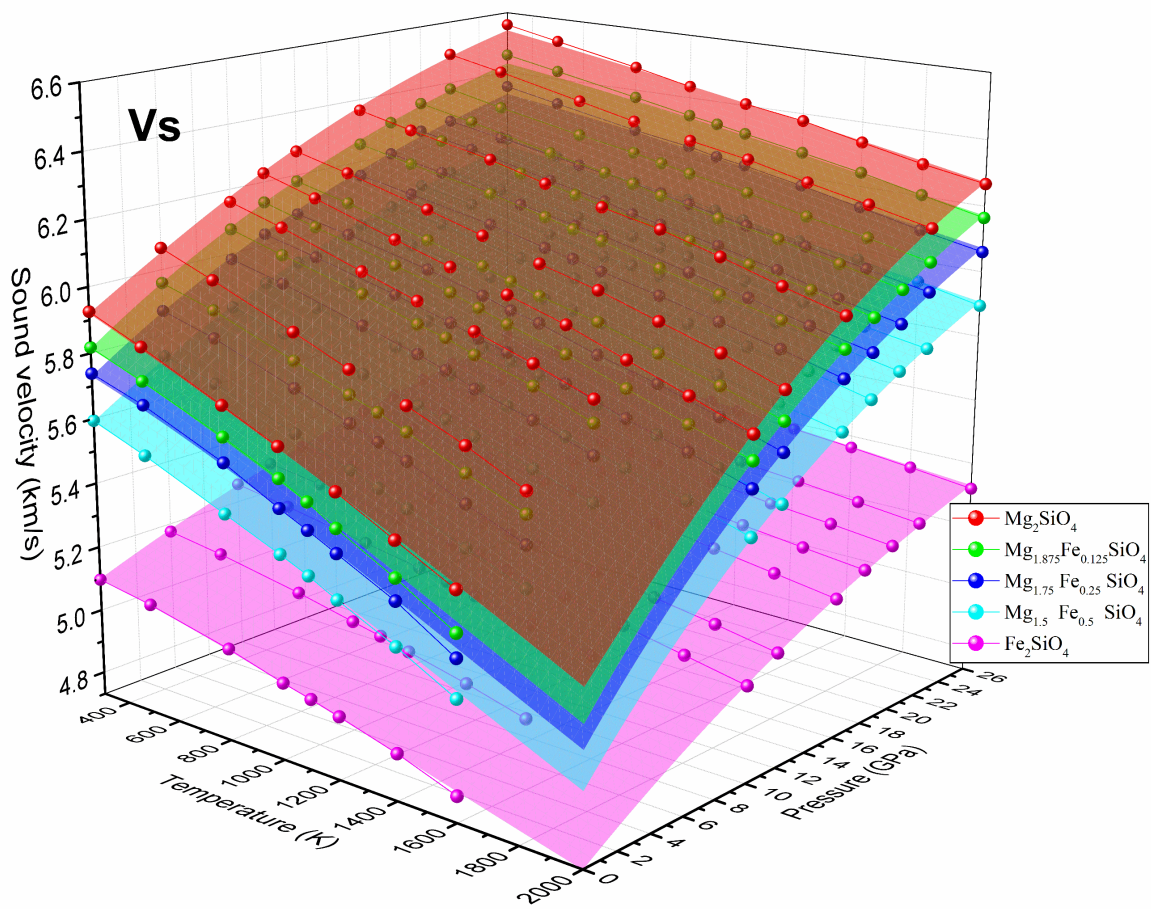
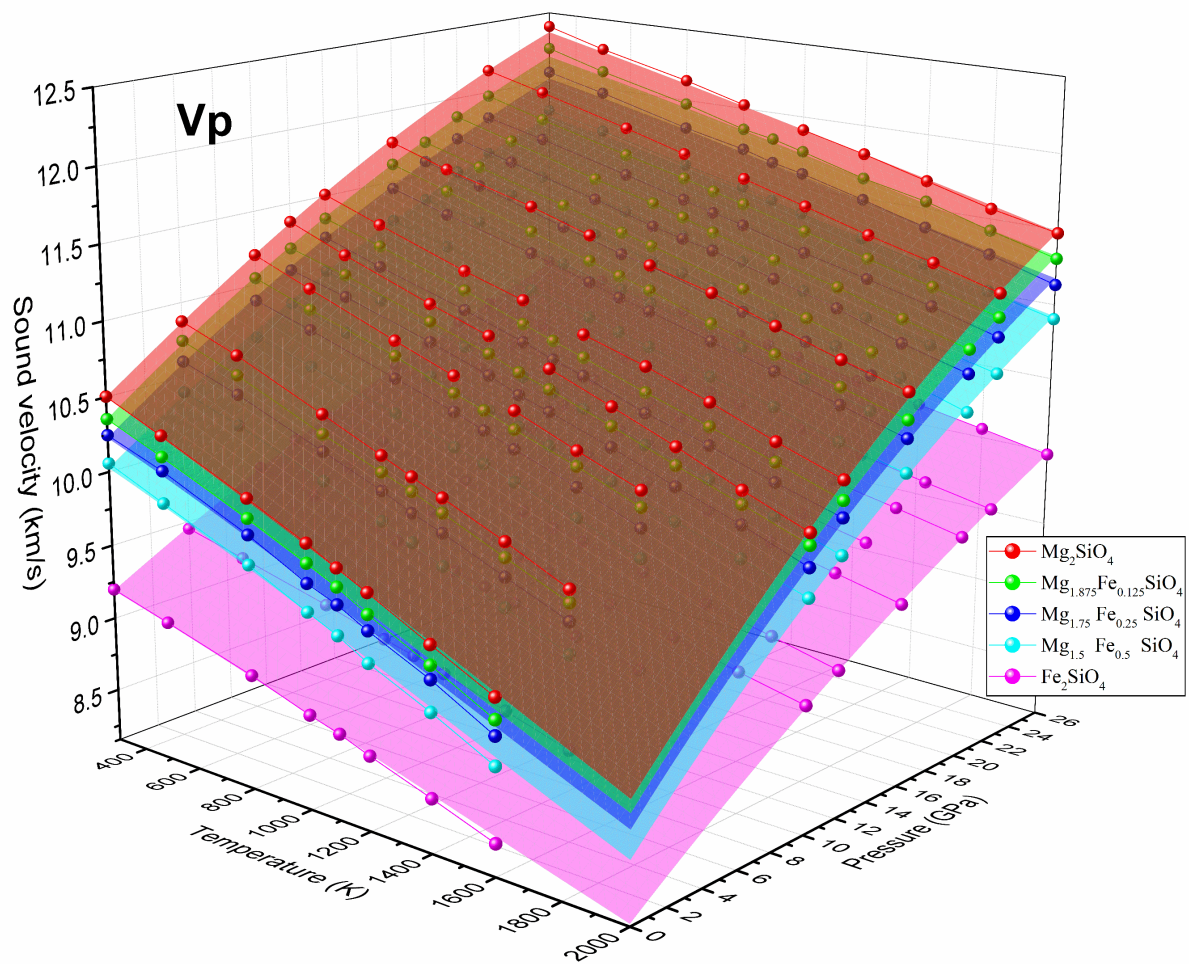


Figure 7.

